

Scalar Split WIMPs and Galactic Gamma-Ray Excess

Karim Ghorbani *

Physics Department, Faculty of Sciences, Arak University, Arak 38156-8-8349, Iran

Hossein Ghorbani[†]

*Institute for Research in Fundamental Sciences (IPM)
School of Particles and Accelerators, P.O. Box 19395-5531, Tehran, Iran*

Abstract

We consider a simple one-component dark matter model with two scalars with a mass splitting δ , interacting with the SM particles through the Higgs portal. We find a viable parameter space consistent with all the bounds imposed by invisible Higgs decay experiments at the LHC, the direct detection experiments by XENON100 and LUX and the dark matter relic abundance provided by WMAP and Planck. We also discuss on the rôle of the co-annihilation and the mass splitting in our computations. Taking into account the constraints above we realize that DM mass less than about 50 GeV is excluded in this model. The model can explain as well the observed gamma-ray excess with $m_{\text{DM}} \sim 63$ GeV and $m_{\text{DM}} \sim 126$ GeV within the analyses of the Fermi-LAT data at high Galactic latitudes, namely, at Galactic latitudes $2^\circ \leq |b| \leq 20^\circ$ and Galactic longitudes $|l| < 20^\circ$, which is referred to as the inner Galaxy.

*kghorbani@ipm.ir

[†]pghorbani@ipm.ir

1 Introduction

Although there is no doubt on the existence of dark matter (DM) which is forming about 26 percent of the matter content of the Universe [1, 2] (see reviews [3, 4]), its fundamental interaction with ordinary matter of the Standard Model (SM) of particle physics is a tremendous mystery in physics today. There is however, a natural explanation for the present value of DM relic density in terms of the thermal freeze-out mechanism of weakly interacting massive particles (WIMPs). Exploiting the WIMP paradigm, a large number of theories beyond the SM is developed with a DM candidate as a WIMP, we name for instance supersymmetric models with R-parity [5, 6, 7, 8, 9] and models with universal extra dimensions [10, 11] as well as models with minimal extension of the SM [12, 13, 14, 15, 16, 17, 18, 19, 20].

All these models can receive stringent constraints on the DM annihilation cross section from Planck [1] and WMAP [2], precise measurements of the DM relic density, and on the WIMP-nucleus scattering cross section from dark matter experiments such as LUX [21] and XENON100 [22]. Moreover, in case of DM production in particle collider experiments like the LHC, measurements on the missing energy and momentum or alternatively on the invisible decay width can put further restrictions on the model parameter space [23, 24, 25, 26].

On the other hand, in light of the recent confirmed observation of the Fermi-LAT extended gamma ray excess, many investigations have directed towards possible explanation of the gamma excess. Assuming that the galactic gamma excess produced as a result of DM annihilation in the galactic center, it is then found in a number of models that DM annihilation cross section of order $\sim 10^{-26} \text{ cm}^3\text{s}^{-1}$ with DM mass in the range 30 – 50 GeV can explain the excess, see as examples [27, 28, 29, 30, 31, 32, 33, 34, 35, 36, 37, 38, 39, 40, 41, 42, 43, 44, 45, 46, 47, 48, 49, 50, 51], and also see [52, 53, 54, 55, 56] for scenarios with lighter DM.

Moreover, recent studies [57, 58, 59] incorporating the systematic uncertainties regarding the Fermi-LAT data analysis, suggest the intriguing possibility to expand the above DM mass to higher values. In fact, they found in [57] that DM mass of $\sim 35 - 165$ GeV decaying into b quark pair and also DM mass large enough to decay into W^+W^- , ZZ , hh , $t\bar{t}$ pairs can be fitted the Fermi data satisfactorily. Moreover, it is found in [59] that larger DM mass up to $m_{\text{DM}} \sim 74$ GeV annihilating into $b\bar{b}$ and also DM annihilation into non-relativistic hh can fit to the data well.

Motivated by these findings, in order to explain the gamma ray excess, it is deemed feasible to investigate models with viable parameter space which excludes DM mass less than ~ 50 GeV.

In this paper we consider a minimal extension of the SM with two additional real scalars, S_1 and S_2 which are SM gauge singlets and interact with the SM particles via a Higgs portal respecting the Z_2 symmetry under which the new scalars are odd and all the SM particles are even. This model suggests two scalar WIMPs, called split WIMPs in [16] where only the light component is stable and the other one is an unstable state. We study this model in detail to find viable region of its parameter space constrained by the limits from the observed DM relic abundance, direct detection bounds and also invisible Higgs decay width bounds when applicable.

Furthermore, we investigate the effect of co-annihilation processes as a distinct feature of the model. We also show that it is possible to find regions in the viable parameter space which can explain the galactic gamma ray excess.

The rest of the paper has the following structure. In section 2 the scalar split model is introduced and relevant free parameters are discussed. Section 3 devoted to calculations on the Higgs decay to two WIMPs and invisible Higgs decay width is provided in terms of the mass range of the DM candidate. In section 4 we calculate the DM annihilation and co-annihilation cross sections and obtain numerically the DM relic density in various parameter setups. The regions in the parameter space are found with sizable contributions from co-annihilation processes. Moreover, the viable parameter space constrained by the DM relic density observation as well as invisible Higgs decay width are studied. Elastic scattering cross section of DM-nucleon is computed as a function of DM mass in section 5, taking into account the limits from relic density observation, direct detection experiments and invisible Higgs decay width. In section 6 we find how it is possible to explain the galactic gamma ray excess within the constrained model parameters. We finish in section 7 with conclusion.

2 Scalar Split WIMPs

We will consider a model for dark matter as a renormalizable extension to the SM with two new real scalar fields denoted by S_1 and S_2 . These new fields may have small mass splitting and transform under Z_2 symmetry as $S_i \rightarrow -S_i$. The full Lagrangian consists of

$$\mathcal{L} = \mathcal{L}_{\text{SM}} + \mathcal{L}_{\text{Dark}} + \mathcal{L}_{\text{int}}. \quad (1)$$

The dark Lagrangian incorporates only the WIMPs particles as

$$\mathcal{L}_{\text{Dark}} = \frac{1}{2}(\partial_\mu S_1)^2 + \frac{1}{2}(\partial_\mu S_2)^2 - \frac{m_1^2}{2}S_1^2 - \frac{m_2^2}{2}S_2^2 - \frac{\lambda_3}{4}S_1^4 - \frac{\lambda_4}{4}S_2^4. \quad (2)$$

In addition, respecting the Z_2 symmetry, WIMPs interaction with the SM particles are considered through a Higgs portal such that

$$\mathcal{L}_{\text{int}}(S_1, S_2, H) = \lambda_1 S_1^2 H^\dagger H + \lambda_2 S_2^2 H^\dagger H + \lambda_{12} S_1 S_2 H^\dagger H. \quad (3)$$

The SM Higgs potential is also given by

$$V_H = \mu_H^2 H^\dagger H + \lambda_H (H^\dagger H)^2. \quad (4)$$

The total potential is then

$$V = V_H + \mathcal{L}_{\text{int}}. \quad (5)$$

The Higgs field is a SM $SU(2)_L$ scalar doublet which develops a non-zero vacuum expectation value (vev) which results in the electroweak spontaneous symmetry breaking. We then parameterize for H as

$$H = \frac{1}{\sqrt{2}} \begin{pmatrix} 0 \\ v + h \end{pmatrix}, \quad (6)$$

where $\langle H \rangle = v = 246$ GeV.

We can choose a basis in which $\langle S_1 \rangle = \langle S_2 \rangle = 0$. The minimization conditions of the total potential are

$$\frac{\partial V}{\partial H}|_{\langle H \rangle = v/\sqrt{2}} = \frac{\partial V}{\partial S_1}|_{\langle S_1 \rangle = 0} = \frac{\partial V}{\partial S_2}|_{\langle S_2 \rangle = 0} = 0. \quad (7)$$

These conditions provide us with some relations between the parameters. We work them out and identify the entries of the mass matrix. From condition $\frac{\partial V}{\partial H}|_{\langle H \rangle} = 0$ we get the relation

$$\mu_H^2 = -\lambda_H v^2. \quad (8)$$

From the other two minimization conditions we get no more relation. We also get the following results for the entries of the mass matrix

$$m_{S_1}^2 = \frac{\partial^2 V}{\partial S_1^2} = m_1^2 + \lambda_1 v^2, \quad m_{S_2}^2 = \frac{\partial^2 V}{\partial S_2^2} = m_2^2 + \lambda_2 v^2, \quad (9)$$

and

$$m_{S_1, S_2}^2 = \frac{\partial^2 V}{\partial S_1 \partial S_2} = \frac{1}{2} \lambda_{12} v^2. \quad (10)$$

We then indicate the two fields H_1 and H_2 as the mass eigenstates by introducing the mass mixing angle θ

$$\begin{aligned} H_1 &= \sin \theta S_1 + \cos \theta S_2, \\ H_2 &= \cos \theta S_1 - \sin \theta S_2, \end{aligned} \quad (11)$$

where,

$$\tan \theta = \frac{y}{1 + \sqrt{1 + y^2}}, \quad \text{with } y = \frac{2m_{S_1, S_2}^2}{m_{S_2}^2 - m_{S_1}^2}. \quad (12)$$

The two neutral scalars H_1 and H_2 have the corresponding mass eigenvalues as

$$m_{H_1, H_2}^2 = \frac{m_{S_1}^2 + m_{S_2}^2}{2} \pm \frac{m_{S_2}^2 - m_{S_1}^2}{2} \sqrt{1 + y^2}. \quad (13)$$

We assume that $m_{H_1} > m_{H_2}$ and therefore H_2 is our stable DM candidate. From eq. (10), eq. (12) and eq. (13) we can express the coupling λ_{12} in terms of the masses m_{H_1} and m_{H_2} and the mass mixing angle θ ,

$$\lambda_{12} = \frac{m_{H_1} - m_{H_2}}{v^2} \frac{y}{\sqrt{1 + y^2}}. \quad (14)$$

We therefore can take in our model seven independent parameters as m_{H_1} , m_{H_2} , λ_{12} , λ_1 , λ_2 , λ_3 , λ_4 , while the mixing angle is then fixed by the relations in eq. (12) and eq. (14).

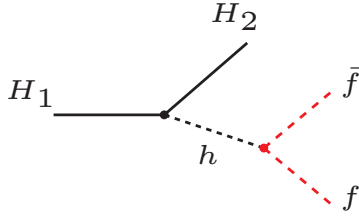


Figure 1: Three body decay of the scalar H_1 into the scalar DM and a fermion pair.

When the small mass splitting is the case then the heavy component WIMP can decay into an off-shell Higgs and the light partner as $H_1 \rightarrow H_2 h$ where h itself decays successively into a fermion pair as $h \rightarrow \bar{f} f$. The Feynman diagram for the decay is shown in Fig. 1.

It is necessary to have an estimate on the life time of the heavy component over the restricted parameter space to know whether or not it has any contribution on the DM relic abundance. Thus for latter use we provide here for the double differential partial decay width of $H_1(k) \rightarrow H_2(p_3) \bar{f}(p_1) f(p_2)$ the formula

$$\frac{d^2\Gamma}{dt du} = \frac{3m_f^2[(\lambda_1 - \lambda_2) \sin 2\theta + \lambda_{12} \cos 2\theta]^2}{128\pi^3 m_{H_1}^3} \left[\frac{t + m_h^2 - m_{H_2}^2 - 4m_f^2}{(t - m_h^2)^2 + \Gamma_h^2 m_h^2} \right], \quad (15)$$

where, the mandelstam variables are $t = (p_1 + p_2)^2$ and $u = (p_2 + p_3)^2$.

3 Invisible Higgs decay

The DM candidate in our model interacts with the SM particles via SM Higgs mediator. It also opens up the possibility for 125 GeV Higgs to decay into the new scalars. Constraints on the model parameters are placed by requiring the invisible Higgs decay to be consistent with the Large Hadron Collider (LHC) measurements. The total decay width of 125 GeV Higgs decaying into SM particles is ~ 4.1 MeV [60] which get enhanced by three invisible decay width of the SM-higgs, $h \rightarrow H_1 H_1$, $h \rightarrow H_1 H_2$ and $h \rightarrow H_2 H_2$. Given an experimental upper limit for the invisible branching ratio for the Higgs boson as $\Gamma_{\text{inv}}/(\Gamma_{\text{inv}} + \Gamma_v) \sim 0.35$ [26] we place a bound on the total invisible decay width as $\Gamma_{\text{inv}}^{\text{total}} < 2.15$ MeV. On the other hand, the total invisible decay width in our model is saturated by three possible decays of Higgs:

$$\Gamma_{\text{inv}}^{11}(h \rightarrow H_1 H_1) = \frac{(\lambda_1 \sin^2 \theta + \lambda_2 \cos^2 \theta + \lambda_{12} \sin \theta \cos \theta)^2}{8\pi m_h} \left(1 - \frac{4m_{H_1}^2}{m_h^2}\right)^{1/2}, \quad (16)$$

$$\Gamma_{\text{inv}}^{22}(h \rightarrow H_2 H_2) = \frac{(\lambda_1 \cos^2 \theta + \lambda_2 \sin^2 \theta - \lambda_{12} \sin \theta \cos \theta)^2}{8\pi m_h} \left(1 - \frac{4m_{H_2}^2}{m_h^2}\right)^{1/2}, \quad (17)$$

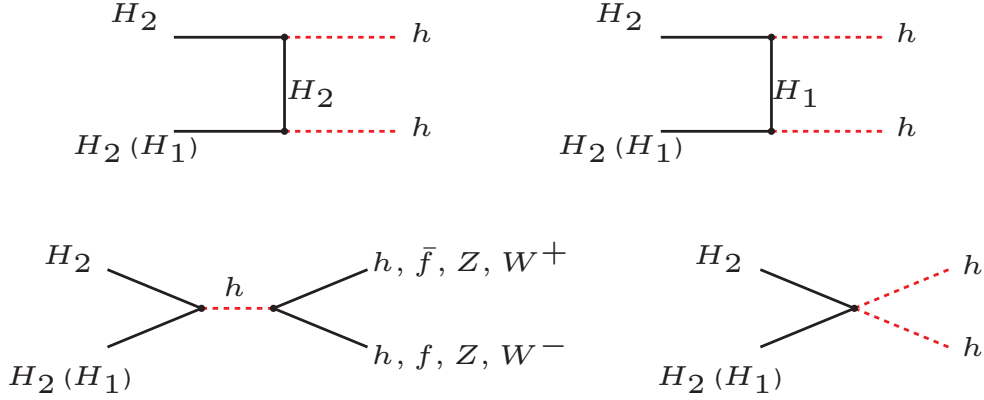


Figure 2: The Feynman diagrams for the DM (co)-annihilation into SM final states.

and

$$\Gamma_{\text{inv}}^{12}(h \rightarrow H_1 H_2) = \frac{[(\lambda_1 - \lambda_2) \sin 2\theta + \lambda_{12} \cos 2\theta]^2}{8\pi m_h^3} \times [m_h^2 - (m_{H_1}^2 + m_{H_2}^2)^2]^{1/2} [m_h^2 - (m_{H_1}^2 - m_{H_2}^2)^2]^{1/2}. \quad (18)$$

Let us define the mass splitting as $\delta \equiv \Delta m_{12} = m_{H_1} - m_{H_2}$. The invisible Higgs decay width depends on DM mass m_{H_2} and δ as the following:

$$\begin{aligned} \Gamma_{\text{inv}}^{\text{total}} &= \Gamma_{\text{inv}}^{22} & \text{when} & \quad \frac{m_h}{2} - \frac{\delta}{2} < m_{H_2} < \frac{m_h}{2}, \\ \Gamma_{\text{inv}}^{\text{total}} &= \Gamma_{\text{inv}}^{22} + \Gamma_{\text{inv}}^{12} & \text{when} & \quad \frac{m_h}{2} - \delta < m_{H_2} < \frac{m_h}{2} - \frac{\delta}{2}, \\ \Gamma_{\text{inv}}^{\text{total}} &= \Gamma_{\text{inv}}^{22} + \Gamma_{\text{inv}}^{12} + \Gamma_{\text{inv}}^{11} & \text{when} & \quad m_{H_2} < \frac{m_h}{2} - \delta. \end{aligned} \quad (19)$$

In section 4 we will show the numerical results.

4 Dark Matter Relic Abundance

Assuming that DM particles have been in thermal equilibrium in the early Universe, the present density of DM depends somehow on the so-called freeze-out temperature, T_f , the epoch in which dark particles become non-relativistic and go out of equilibrium. At freeze-out temperature the annihilation rate of DM falls off below the Hubble expansion rate and on the other side, due to the low budget of the kinetic energy, the DM production reactions get suppressed. The relic density of DM is achievable by solving the Boltzmann equation(s) for the time evolution of DM number density, n_{DM} . In the model under consideration, there are two new scalars beside the SM particles that their number density evolutions are relevant in order to obtain the DM relic abundance. We assumed that H_2 is the light component and thus being stable. We therefore consider H_2 as our DM candidate with mass m_{H_2} that $m_{H_1} > m_{H_2}$. It therefore can undergo the decay $H_1 \rightarrow H_2 + \text{SM}$.

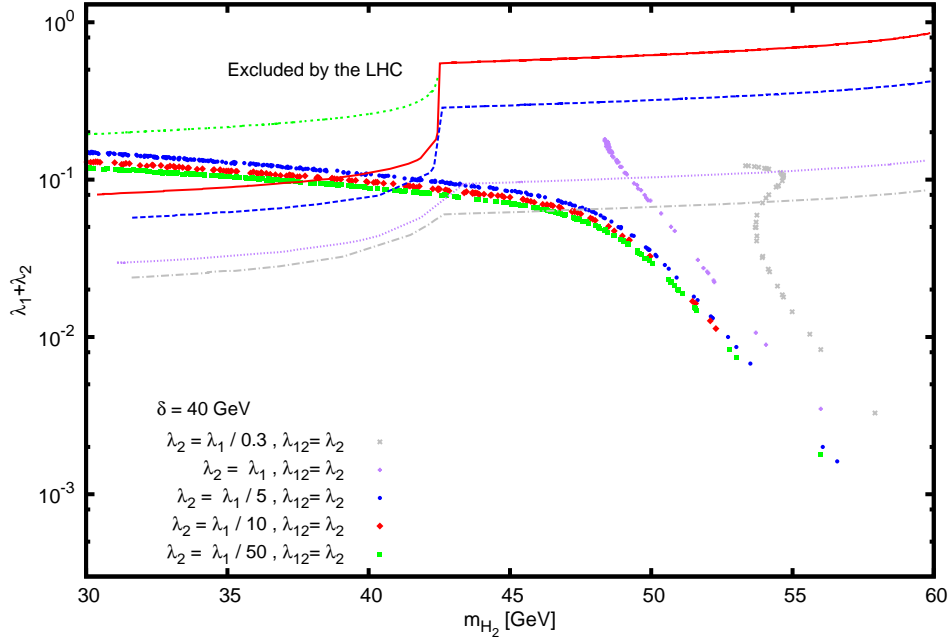


Figure 3: The viable parameter sets are obtained in the plane $(\lambda_1 + \lambda_2, m_{H_2})$ using constraints from the relic density observation and invisible decay width. For each set of parameters the lower bound from invisible Higgs decay width are placed for $m_{H_2} < m_h/2$, indicated by dashed line with respective color. The mass splitting is $\delta = 40$ GeV.

Annihilation reactions are one type of processes that change the number density (n_1 and n_2) of our species here. The possible annihilations of H_1 and H_2 to SM particles are depicted in Fig. 2. As it is evident from the Feynman diagrams, annihilation reactions into SM fermion pairs, W^+W^- and ZZ occur via s channel while annihilation into SM-Higgs pair is possible through s -, t - and u -channel. An annihilation process in which DM particle annihilates together with H_1 is the so-called co-annihilation reaction. Another type of reaction that changes the number density is the decay process of the heavier component, i.e., H_1 . The abundance of H_1 and H_2 are determined by solving two coupled Boltzmann equations,

$$\begin{aligned} \frac{dn_1}{dt} = & -3Hn_\chi - \langle\sigma_{11}v_{11}\rangle[n_1n_1 - (n_1^{\text{eq}}n_1^{\text{eq}})] - \langle\sigma_{12}v_{12}\rangle[n_1n_2 - (n_1^{\text{eq}}n_2^{\text{eq}})] \\ & - \Gamma_{12}(n_1 - (n_1^{\text{eq}})), \end{aligned} \quad (20)$$

and

$$\begin{aligned} \frac{dn_2}{dt} = & -3Hn_\chi - \langle\sigma_{21}v_{21}\rangle[n_2n_1 - (n_2^{\text{eq}}n_1^{\text{eq}})] - \langle\sigma_{22}v_{22}\rangle[n_2n_2 - (n_2^{\text{eq}}n_2^{\text{eq}})] \\ & + \Gamma_{12}(n_1 - (n_1^{\text{eq}})), \end{aligned} \quad (21)$$

where $\langle\sigma v\rangle$ indicates thermal average over *annihilation cross section* \times *relative ve-*

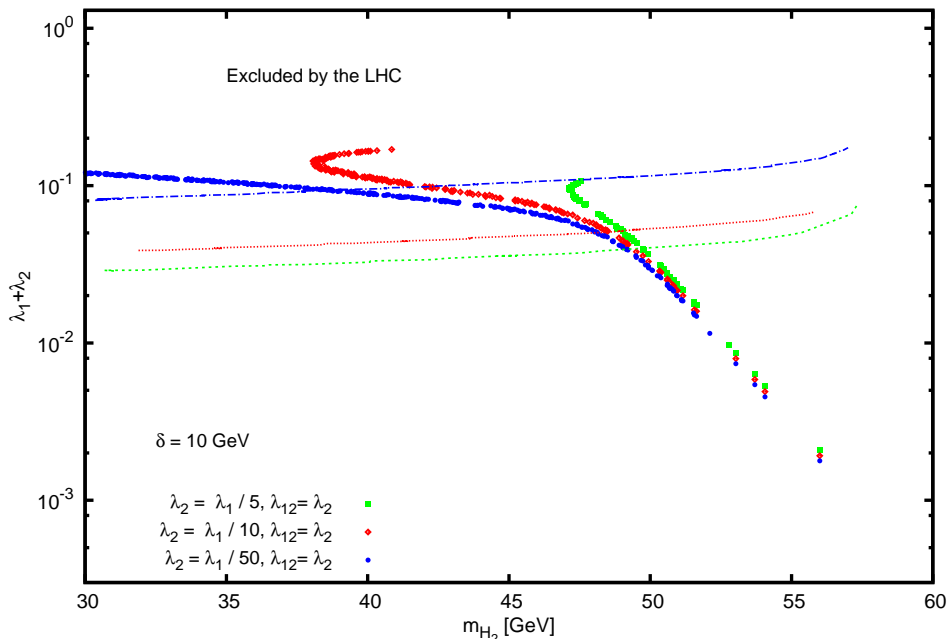


Figure 4: As in Fig. 3 with mass splitting $\delta = 10$ GeV.

locity at temperature T . In appendix A we present our formulas for annihilation cross sections of dark matter candidate in three possible channels. To confirm our analytical formula we employ the program CalcHEP [61] which in turn requires implementation of our model into the program LanHEP [62]. To perform our analysis for the DM relic abundance we need to solve numerically the two Boltzmann equations simultaneously. To this end, we utilize the program MicrOMEGAs [63] for our model.

Let us begin now with our probe over the parameter space of the model. As explained earlier we have two choices for a set of independent parameters we would like to place our constraints on. One possibility is the set $\{m_{H_1}, m_{H_2}, \lambda_1, \lambda_2, \lambda_{12}\}$ and the other option is the set $\{m_{H_1}, m_{H_2}, \lambda_1, \lambda_2, \theta\}$. In our analysis we choose the first set and apply the relation in eq. (14) to obtain the corresponding mixing angle θ . We also notice that the couplings λ_3 and λ_4 do not show up in DM annihilation cross sections and thus are not relevant in our analysis. To proceed we start with the mass splitting $\delta = 40$ GeV and generate random values for DM mass with $30 \text{ GeV} < m_{H_2} < m_h/2$ and $0 < \lambda_1 < 1$. Using the combined result from WMAP and Planck for the present DM relic density, our results exhibited in Fig. 3 show the viable parameter space for different set of values for the couplings λ_2 and λ_{12} . For DM mass below $m_h/2$, only DM annihilation into fermions mediated via SM-Higgs are potentially allowed processes, thus one expects enhancement on the cross section near the SM-Higgs mass resonance. This feature is depicted in Fig. 3 such that for larger values of DM mass up to $m_{H_2} \sim 60$ GeV, smaller values of λ_1 and therefore λ_2 are picked out to compensate for the enhanced cross section. Moreover, we place in

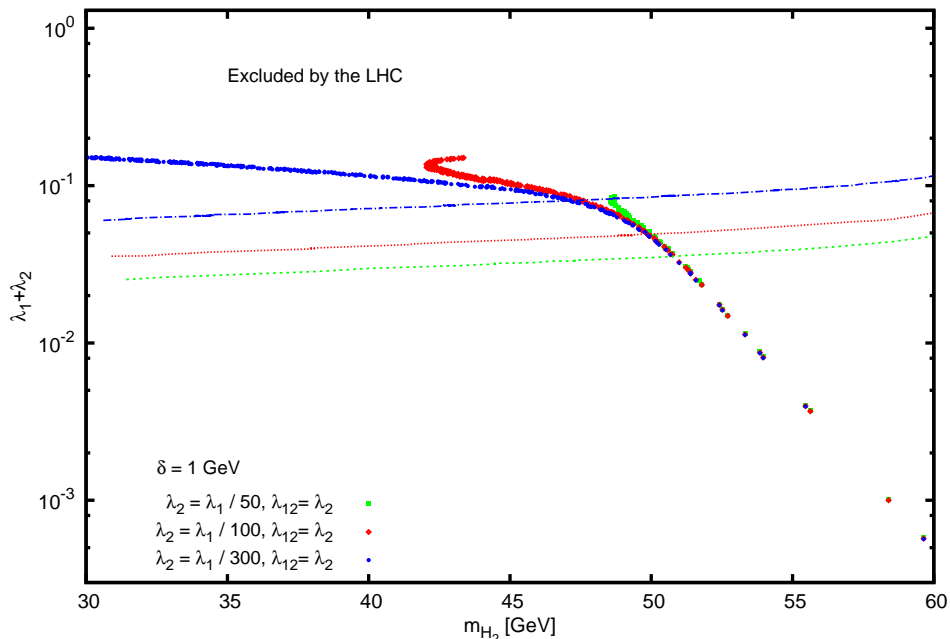


Figure 5: As in Fig. 3 with mass splitting $\delta = 1$ GeV.

Fig. 3 the lower limit for the coupling λ_1 in the plane $(\lambda_1 + \lambda_2, m_{H_2})$ by respecting the upper value for the invisible Higgs decay width obtained at the LHC. One notices here that for mass splitting as large as 40 GeV, a region in the parameter space with $m_{H_2} < 60$ GeV can be found which respects both relic density abundance and invisible Higgs decay width. We then continue with doing the same analysis but with smaller mass splitting $\delta = 10$ GeV and show in Fig. 4 our numerical results. With this mass splitting we realize that DM mass less than ~ 40 GeV is excluded by the invisible Higgs decay width when $\lambda_2 = \lambda_1/50$. Finally, our analysis illustrated in Fig. 5 in the case of mass splitting $\delta = 1$ GeV indicates that DM candidate with mass less than ~ 47 GeV is excluded by the LHC bound on the invisible Higgs decay width.

We summarize our findings up to this point by this observation that the bounds from invisible Higgs decay width becomes increasingly strong with lowering δ .

We next turn to an analysis in connection with the size of the co-annihilation contributions in the relic abundance within the aforementioned model, see [64] for general discussions on the co-annihilation. In this regards, the off-diagonal coupling λ_{12} , λ_1 and λ_2 play an important role because after diagonalizing the mass matrix, these couplings determine the strength of the WIMPs interaction vertex hH_1H_2 . We study two distinct cases for the ordering of the couplings: $\lambda_1 < \lambda_{12}$ and $\lambda_1 > \lambda_{12}$. First we look at the condition when $\lambda_1 = \lambda_{12}/3$ and $\lambda_2 = \lambda_{12}$. Our results for the co-annihilation effects with the mass splitting $\delta = 10$ GeV are shown in Fig. 6 and with $\delta = 1$ GeV are exhibited in Fig. 7.

It can be seen from the figures that taking into account the co-annihilation pro-

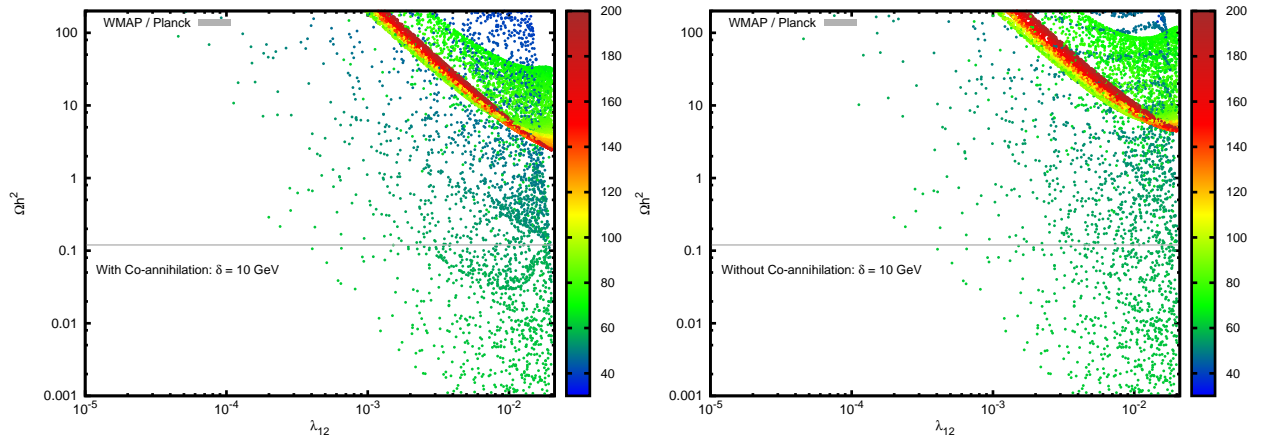


Figure 6: DM Relic density as a function of the coupling λ_{12} with $\delta = 10$ GeV. Left panel: Both annihilation and co-annihilation processes are taken into account. Right panel: Only annihilation reactions are considered. For the couplings we have $\lambda_1 = \lambda_{12}/3$ and $\lambda_2 = \lambda_{12}$. The vertical color spectrum indicates range of the DM mass.

cesses they result in a significant reduction of the relic density for both mass splittings. Therefore, one should not discount the contributions of the co-annihilation processes on the relic density for a wide range of the DM mass, almost irrespective of the size of λ_{12} . Moreover, we study another avenue in which chosen are $\lambda_1 = 3\lambda_{12}$ and $\lambda_2 = \lambda_{12}$. We present our results in Fig. 8 and Fig. 9 for mass splitting $\delta = 10$ GeV and $\delta = 1$ GeV, respectively. In this case it turns out a rather different behavior from the co-annihilation contributions. For the larger mass splitting there is almost no effect of co-annihilation on the relic abundance but there can be seen small enhancement on the relic density due to the co-annihilation processes.

It is interesting that within our model there can be found regions in the parameter space that even for small mass splitting the presence of co-annihilation reactions are almost ineffective while in another region these effects are sizable. Moreover, within our model we reach to this conclusion that relic density is allowed to increase or decrease due to the inclusion of co-annihilation, depending on the region of parameter space we probe. The latter feature is already observed in supersymmetry model, see discussions in [65, 66]. It is also found in [67, 68, 69, 70] that the effect of co-annihilation is important in models with Universal Extra Dimension and in fact, the final effect is to increase the relic abundance of the lightest Kaluza-Klein particle. It is also shown that within a radiative seesaw model the co-annihilation effects cause an increase in the relic density [71].

We should emphasize here that within the parameter space scanned in this section and also that in the next section, by computing numerically the decay life time of the heavy WIMP using the relation in eq. (15) we ensure the life time of the heavy scalar is by far smaller than the age of the Universe and therefore cannot contribute to the DM relic abundance.

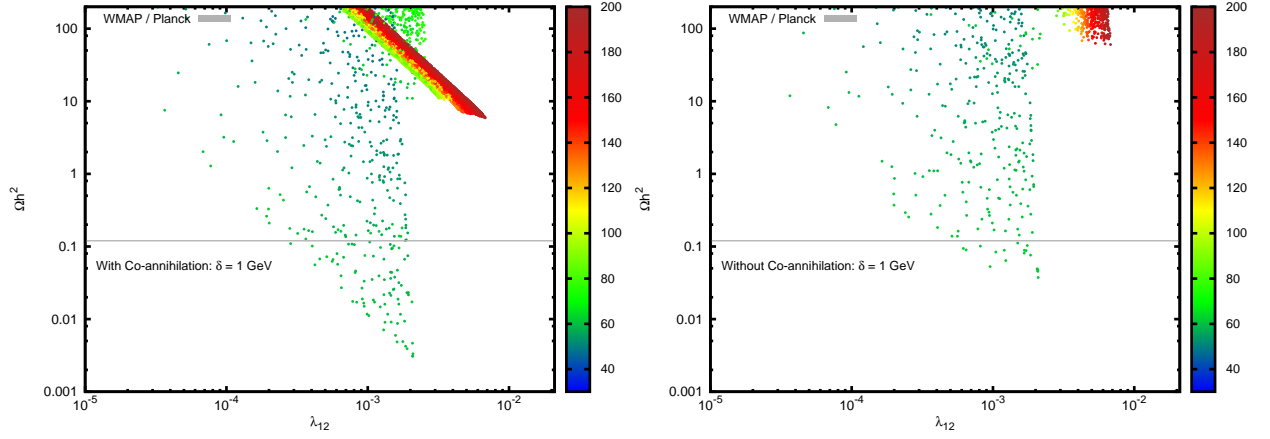


Figure 7: DM Relic density as a function of the coupling λ_{12} with $\delta = 1$ GeV. Left panel: Both annihilation and co-annihilation processes are taken into account. Right panel: Only annihilation reactions are considered. For the couplings we have $\lambda_1 = \lambda_{12}/3$ and $\lambda_2 = \lambda_{12}$. The vertical color spectrum indicates range of the DM mass.

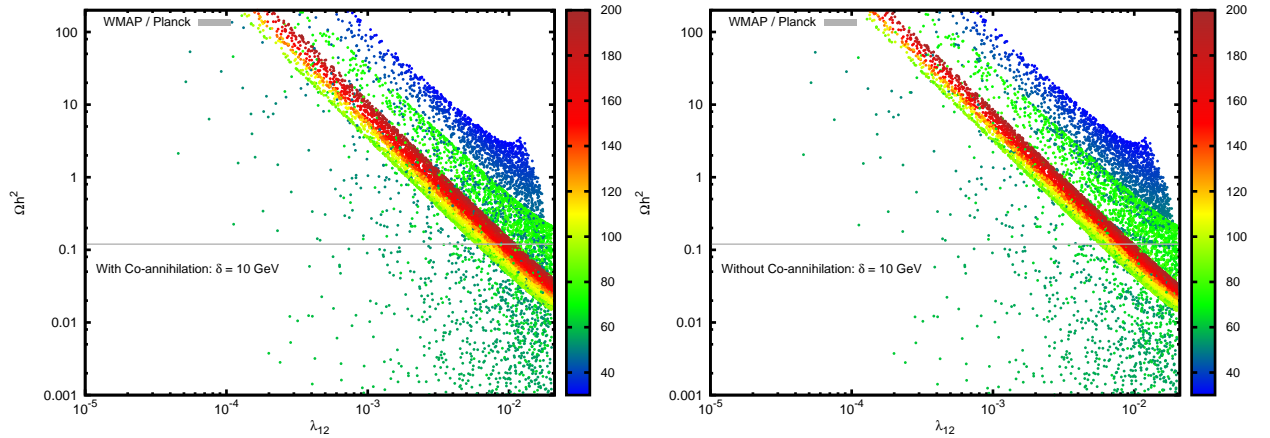


Figure 8: DM Relic density as a function of the coupling λ_{12} with $\delta = 10$ GeV. Left panel: Both annihilation and co-annihilation processes are taken into account. Right panel: Only annihilation reactions are considered. For the couplings we have $\lambda_1 = 3\lambda_{12}$ and $\lambda_2 = \lambda_{12}$. The vertical color spectrum indicates range of the DM mass.

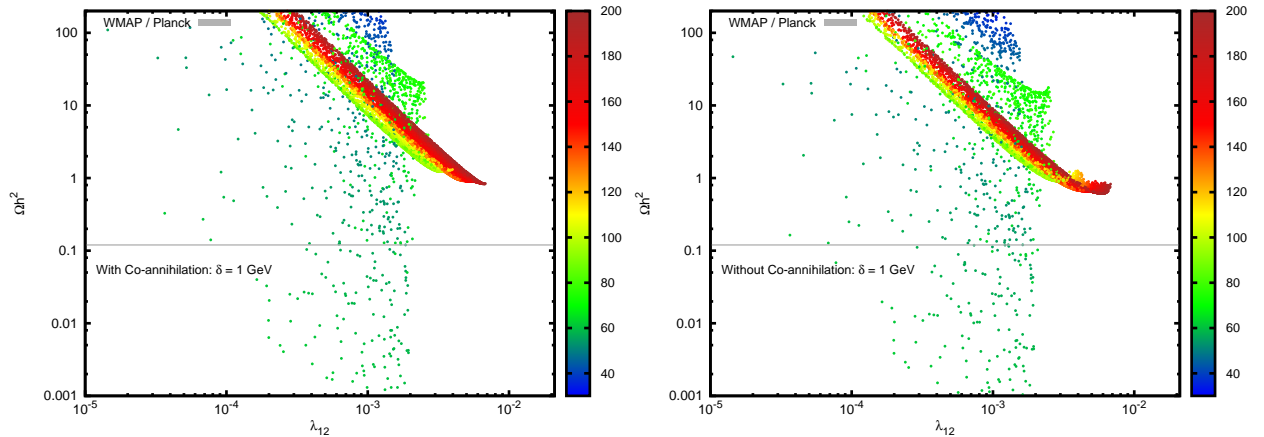


Figure 9: DM Relic density as a function of the coupling λ_{12} with $\delta = 1$ GeV. Left panel: Both annihilation and co-annihilation processes are taken into account. Right panel: Only annihilation reactions are considered. For the couplings we have $\lambda_1 = 3\lambda_{12}$ and $\lambda_2 = \lambda_{12}$. The vertical color spectrum indicates range of the DM mass.

5 Direct detection

Direct detection experiments are designed to study the unknown nature of DM interaction with ordinary matter. In these experiments the attempt is to measure the enticing event rate for the DM scattering off the target nuclei in the detector. Although the present results from DM experiments such as LUX [21] and XENON100 [22] show no evidence for DM interactions, they offer an impressive upper bound on the spin-independent DM-nucleon elastic scattering cross section. We will apply these findings in the following to constrain further the parameter space of our model which is already restricted by the limits from WMAP and Planck.

To this end, we need to calculate the elastic scattering of WIMP-nucleon. In our particular model the interaction of DM with nucleon occurs through a fundamental interaction of DM with quark which is mediated by the SM-Higgs, where the relevant Feynman diagram depicted in Fig. 10. The effective Lagrangian responsible for the DM-quark interaction is

$$\mathcal{L}_{\text{eff}} = \alpha_q H_2 H_2 \bar{q} q, \quad (22)$$

where, the coupling α_q is given by

$$\alpha_q = \frac{m_q}{m_h^2} (\lambda_1 \cos^2 \theta + \lambda_2 \sin^2 \theta - \lambda_{12} \sin \theta \cos \theta). \quad (23)$$

To find the elastic scattering cross section we can invoke the assumption that in the limit of vanishing momentum transfer it is possible to replace the nucleonic matrix element including quark current with that containing nucleon current up to some proportionality factor [72, 73, 74, 75], see also [76]. We arrive at the final result for

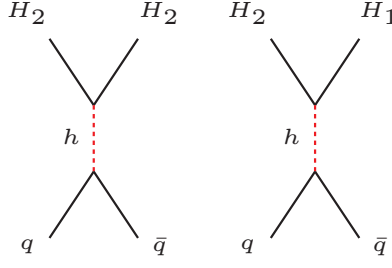


Figure 10: The relevant Feynman diagrams for the WIMP-nucleon scattering.

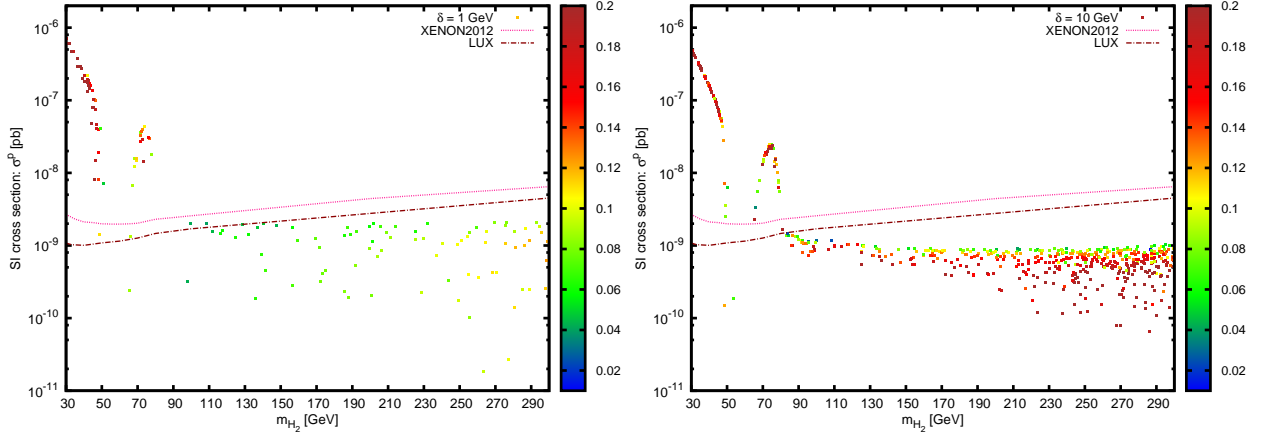


Figure 11: Spin independent elastic scattering cross section of DM with nucleon are shown as a function of the DM mass and comparison has made with the latest results from LUX and XENON experiments. In the left panel chosen for the mass splitting is $\delta = 1$ GeV and in the right panel it is $\delta = 10$ GeV. The vertical color spectrum indicates the size of $\lambda_1 + \lambda_2$.

the spin-independent (SI) cross section of DM-nucleon as

$$\sigma_{\text{SI}}^{\text{N}} = \frac{\alpha_N^2 \mu_N^2}{\pi m_{\text{DM}}^2}, \quad (24)$$

where μ_N is the reduced mass of the DM-nucleon system and the factor α_N depends on the scalar couplings f_{Tq}^N and f_{Tg}^N as

$$\alpha_N = m_N \sum_{q=u,d,s} f_{Tq}^N \frac{\alpha_q}{m_q} + \frac{2}{27} f_{Tg}^N \sum_{q=c,b,t} \frac{\alpha_q}{m_q}. \quad (25)$$

We use in our numerical calculations the following values for the scalar couplings

$$f_u^p = 0.0153, \quad f_d^p = 0.0191, \quad f_s^p = 0.0447. \quad (26)$$

We report on our numerical results for the elastic scattering of DM-proton in Fig. 11 and Fig. 12, considering three different mass splittings, namely $\delta = 1$ GeV,

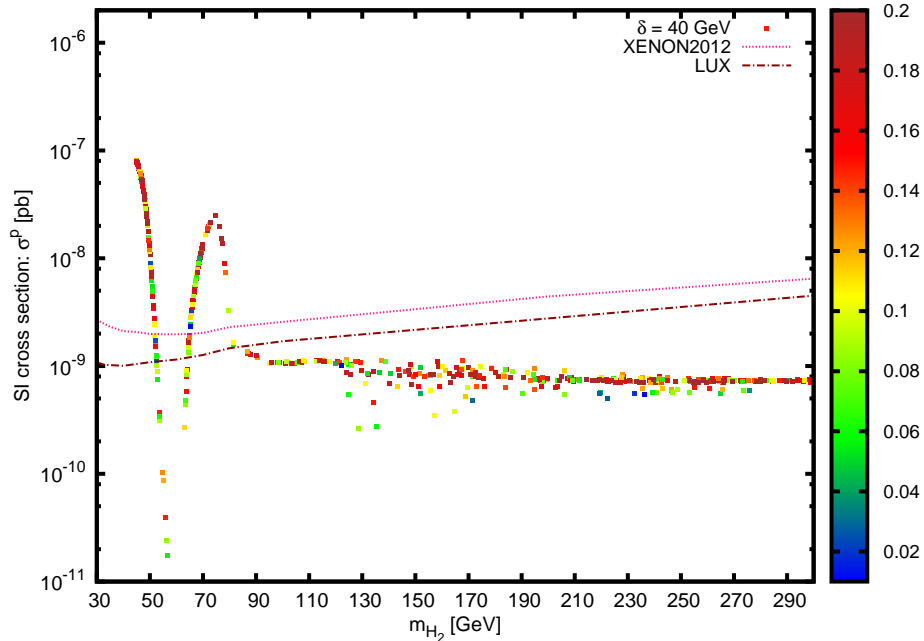


Figure 12: Same as Fig. 11 but with $\delta = 40$ GeV.

$\delta = 10$ GeV and $\delta = 40$ GeV. One can readily see from the figures that DM mass smaller than about 50 GeV is excluded by LUX and XENON bound for the above mass splittings. On the other side, there can be found viable region with DM mass larger than ~ 80 GeV in case $\delta = 10$ GeV and $\delta = 40$ GeV and viable parameter space with DM mass larger than ~ 90 GeV when $\delta = 1$ GeV. It is worth mentioning that when chosen is $\delta = 40$ GeV, the viable region in the parameter space with DM mass between 50 GeV and 65 GeV which respect the LUX and XENON data is more plausible.

Having discussed the scalar split WIMPs, there is a possibility of inelastic scattering interaction between the dark matter particle and the nucleus that we have not considered in our computations till this point. The contribution of the inelastic scattering can be as important as the elastic scattering in the split WIMPs models and should be summed up before comparing with the experimental data. In general, for multi-component dark matter models that in the present Universe there exist more than one stable dark matter particle, the inelastic interaction can occur in two processes; endothermic process where the lighter component scatters into heavier one, and the exothermic process where the heavier component turns into the lighter dark matter component. In our model the relevant inelastic scattering is the endothermic reaction; i.e. the stable (lighter) scalar H_2 through the nucleus, scatters into H_1 , and subsequently H_1 decays into SM particles (see Fig. 10). However, for large WIMPs mass splitting δ it can be shown that the kinematics forbids the first-order inelastic scattering, see e.g. ([77]). For our model inelastic WIMP-nucleon interaction begins contributing for $\delta \sim \text{KeV}$ which is far smaller from the limits we have considered in this work i.e. $\delta \sim \text{GeV}$.

6 Gamma-ray emission from DM annihilation

The analysis of Fermi Large Area Telescope (Fermi-LAT) data [78] (see [79] for the recent report) triggered by Goodenough and Hooper [80, 81] and continued by several groups [57, 58, 82, 83, 84, 85, 86, 87, 88, 89] revealed an excess in the gamma-rays from the center of the Milky Way or Galaxy Center (GC), hence dubbed Galactic Center Excess (GCE). The gamma-ray emission produced by the millisecond pulsars in the galaxy center can only contribute in 5-10% of the excess observed [90]. Other sources such as cosmic ray interactions are disfavored as well [91].

On the other hand, surprisingly the morphology and the spectrum of the GCE is well fitted when the dark matter annihilation into standard model particles is added in the background model used in the analyses. All diffuse background models where include the WIMP as a component agree in morphology. However, the position of the gamma-ray peak in the energy spectrum and the mass of the dark matter annihilating into SM particles varies by considering the systematic uncertainties in the background model [57, 58].

The dark matter candidate depending on its mass can annihilate into leptons, the quarks, the gauge bosons and the Higgs. The gamma-ray is then produced through the cascade decays of these particles to neutral pion by the hadronization of the quarks, also through the bremsstrahlung of the charged gauge bosons and leptons. Among these processes the gamma-rays from the pion decay is dominated compared with the gamma emission from bremsstrahlung. The differential gamma-ray flux produced by a single W , Z , Higgs boson and top quark is depicted in Fig. 1 of [57]. It can be easily seen that the peak of the spectrum is moving towards the higher energies for heavier particles.

It was believed formerly (see e.g.[86, 88]) that dark matter candidates with masses being only in the range of $30 \text{ GeV} < m_{\text{DM}} < 50 \text{ GeV}$ decaying into $\bar{b}b$ give an acceptable fit with the excess observed in the Fermi data. In the recent works however it is argued that taking into account the systematic uncertainties in the analysis of the Fermi data not only the mass range of dark matter for $\bar{b}b$ channel is enlarged to $35 \text{ GeV} < m_{\text{DM}} < 165 \text{ GeV}$ but also larger dark matter masses in annihilation to WW , ZZ , hh , and $t\bar{t}$ can be fitted well with the data [57]. Additionally, it is pointed out in [59] that DM mass up to about 74 GeV decaying into b quark pair and also DM annihilation into non-relativistic hh can fit the Fermi data well.

We show that the gamma-ray excess in our scalar WIMPs model can be explained well. To this end, we obtain the photon flux produced by dark matter annihilation which is consistent with the parameter space we have confined already in the last sections by looking at direct detection, relic density and LHC bounds.

The gamma-ray flux is determined in terms of the annihilation cross section $\langle\sigma v\rangle_{\text{ann}}$, the mass of the annihilating dark matter m_{DM} , the gamma-ray spectrum generated per annihilation dN_γ/dE_γ and the density of dark matter ρ in the region of interest (ROI) which is the GC:

$$\frac{d^2\Phi}{dE_\gamma d\Omega} = \frac{1}{16\pi} \frac{\langle\sigma v\rangle_{\text{ann}}}{m_{\text{DM}}^2} \frac{dN_\gamma}{dE_\gamma} \int_0^\infty dr \rho^2(r), \quad (27)$$

The density of dark matter in the Milky Way galaxy is assumed to be spherically

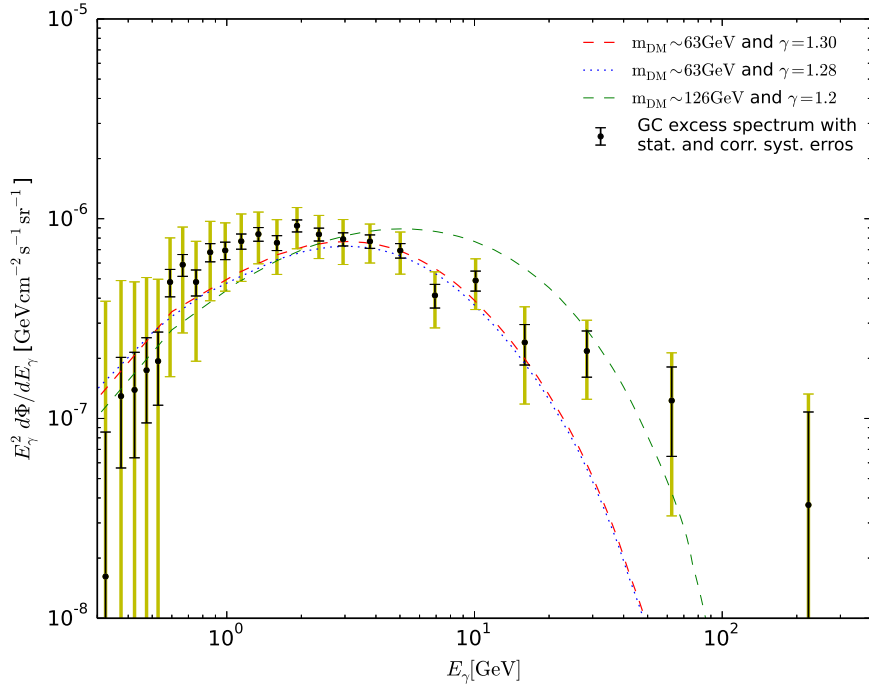


Figure 13: Shown is the gamma-ray flux multiplied by energy squared from annihilating dark matter computed in our scalar split WIMPs model for dark matter mass $m_{\text{DM}} \sim 63$ GeV and also dark matter mass $m_{\text{DM}} \sim 126$. The black error bars accompanied with correlated systematic errors is the obtained flux from Fermi-LAT data [58].

symmetric. The density distribution is then a function of r and is described by the generalized Navarro-Frenk-White (NFW) halo profile [92]:

$$\rho(r) = \rho_{\odot} \left(\frac{r_{\odot}}{r} \right)^{\gamma} \left(\frac{r_s + r_{\odot}}{r_s + r} \right)^{3-\gamma}, \quad (28)$$

where $r_s = 20$ kpc is the scale radius, $\rho_{\odot} = 0.3$ GeV/cm³ is the local dark matter density at $r_{\odot} = 8.5$ kpc and r is the distance from the center of the galaxy to the point where the dark matter annihilation occurs. The parameter γ is the slope parameter being $\gamma = 1$ for the standard NFW. In our calculations we take γ within the interval $\gamma = 1.2 - 1.3$ used in the literature.

We find out that within the parameter space confined by relic density and direct detection in our DM model, there can be found regions producing gamma excess that are compatible with the fluxes provided by the Fermi data. We have used micrOMEGAs package for computation of gamma-ray flux in our particular model with dark matter masses $m_{\text{DM}} \sim 63$ GeV and $m_{\text{DM}} \sim 126$ GeV where the mass splitting is $\delta = 40$ GeV.

In Fig. 13 we present our results for the gamma-ray flux multiplied by the gamma energy squared. In this figure it is shown the prediction of the scalar split WIMPs model for the gamma excess from annihilating dark matter of mass ~ 63 GeV with the total annihilation cross section $\langle \sigma \rangle_{\text{ann}} \sim 4.6 \times 10^{-26} \text{cm}^3 \text{s}^{-1}$ and from DM mass ~ 126 GeV with total annihilation cross section $\langle \sigma \rangle_{\text{ann}} \sim 2 \times 10^{-25} \text{cm}^3 \text{s}^{-1}$ to be compared with the excess observed from the Fermi-LAT data. Comparison made with the data analysis provided by [58] at high Galactic latitudes $2^\circ \leq |b| \leq 20^\circ$ indicates the validity of the current model in explaining the Galactic gamma excess.

7 Conclusions

In this paper we have employed a simple model of dark matter called Scalar Split WIMPs with two scalars H_1 and H_2 interacting with SM particles through the Higgs portal. Depending on the mass splitting $\delta = m_{H_1} - m_{H_2}$ and the couplings in the model, the decay rate of the heavier scalar H_1 , $m_{H_1} > m_{H_2}$ varies. For the parameter space we exploit in this work the H_1 decay rate is much smaller than the age of the Universe. Therefore we have only one scalar H_2 that contribute in the DM relic abundance, although the co-annihilation plays a rôle in the value of the relic density.

We have examined our model with four observational and experimental bounds imposed by invisible Higgs decay, the amount of dark matter abundance, the limits put on nucleus-DM cross sections by direct detection experiments, and the gamma excess found by analyses in the Fermi-LAT data.

The model possesses seven free parameters out of which only five parameters m_{H_1} , m_{H_2} , λ_1 , λ_2 , λ_{12} enter into the annihilation cross section computations. One critical parameter that can change the viable parameter space in various computations is the mass splitting δ . It has been shown that lowering the mass splitting δ puts strong bounds on the invisible Higgs decay widths. We have also explored the rôle of the co-annihilation processes for different mass splittings in the computation of

the relic density using only the parameter space already compatible with the LHC invisible Higgs decay widths. The relic density gets affected by the co-annihilation when changing the mass splitting. Figs. 6-9 reflect such an effect.

Our model successfully passes all the above constraints and in particular predicts a gamma-ray excess which is in agreement in morphology and spectrum with the excess observed out of Fermi data. To compute the gamma-ray flux which is produced by bremsstrahlung processes and the pion decay created from cascade annihilations of dark matter into SM final states, we have used the so-called NFW halo profile for the dark matter density at high Galactic latitudes of the galaxy.

A Annihilation cross sections

The annihilation cross sections into fermion pairs for the dark matter candidate, H_2 is

$$\sigma_{\text{ann}} v_{\text{rel}}(\bar{H}_2 H_2 \rightarrow \bar{f} f) = \frac{N_c m_f^2}{\pi} \left(1 - \frac{4m_f^2}{s}\right)^{\frac{3}{2}} \left[\frac{(\lambda_1 \cos^2 \theta + \lambda_2 \sin^2 \theta - \lambda_{12} \sin \theta \cos \theta)^2}{(s - m_h^2)^2 + m_h^2 \Gamma_h^2} \right], \quad (29)$$

and for annihilation into gauge bosons W^\pm and Z is

$$\sigma_{\text{ann}} v_{\text{rel}}(\bar{H}_2 H_2 \rightarrow \bar{W}^+ W^-, ZZ) = \frac{1}{2\pi s} \left[\frac{(\lambda_1 \cos^2 \theta + \lambda_2 \sin^2 \theta - \lambda_{12} \sin \theta \cos \theta)^2}{(s - m_h^2)^2 + m_h^2 \Gamma_h^2} \right] \times \\ \left[((s - 2m_W^2)^2 + 8m_W^2) \left(1 - \frac{4m_W^2}{s}\right)^{\frac{1}{2}} + \frac{1}{2} ((s - 2m_Z^2)^2 + 8m_Z^2) \left(1 - \frac{4m_Z^2}{s}\right)^{\frac{1}{2}} \right]. \quad (30)$$

References

- [1] P. A. R. Ade *et al.* [Planck Collaboration], *Astron. Astrophys.* **571** (2014) A16 [arXiv:1303.5076 [astro-ph.CO]].
- [2] G. Hinshaw *et al.* [WMAP Collaboration], *Astrophys. J. Suppl.* **208** (2013) 19 [arXiv:1212.5226 [astro-ph.CO]].
- [3] G. Bertone, D. Hooper and J. Silk, *Phys. Rept.* **405** (2005) 279 [hep-ph/0404175].
- [4] L. Bergstrom, *Rept. Prog. Phys.* **63** (2000) 793 [hep-ph/0002126].
- [5] K. Choi, K. Y. Lee, Y. Shimizu, Y. G. Kim and K. i. Okumura, *JCAP* **0612** (2006) 017 [hep-ph/0609132]. ;
- [6] T. Moroi and L. Randall, *Nucl. Phys. B* **570** (2000) 455 [hep-ph/9906527].
- [7] G. Jungman, M. Kamionkowski and K. Griest, *Phys. Rept.* **267** (1996) 195;
- [8] J. R. Ellis, J. S. Hagelin, D. V. Nanopoulos, K. A. Olive and M. Srednicki, *Nucl. Phys. B* **238** (1984) 453. ;
- [9] H. Goldberg, *Phys. Rev. Lett.* **50** (1983) 1419 [Erratum-ibid. **103** (2009) 099905].;

- [10] H. C. Cheng, J. L. Feng and K. T. Matchev, Phys. Rev. Lett. **89** (2002) 211301 [hep-ph/0207125]. ;
- [11] G. Servant and T. M. P. Tait, Nucl. Phys. B **650** (2003) 391 [hep-ph/0206071].
- [12] V. Silveira and A. Zee, Phys. Lett. B **161** (1985) 136. ;
- [13] C. P. Burgess, M. Pospelov and T. ter Veldhuis, Nucl. Phys. B **619** (2001) 709 [hep-ph/0011335].
- [14] J. McDonald, Phys. Rev. D **50** (1994) 3637 [hep-ph/0702143 [HEP-PH]].
- [15] M. Cirelli, N. Fornengo and A. Strumia, Nucl. Phys. B **753** (2006) 178 [hep-ph/0512090].
- [16] M. Pospelov and A. Ritz, Phys. Rev. D **84** (2011) 113001 [arXiv:1109.4872 [hep-ph]].
- [17] L. Lopez-Honorez, T. Schwetz and J. Zupan, Phys. Lett. B **716** (2012) 179 [arXiv:1203.2064 [hep-ph]].
- [18] V. Barger, P. Langacker, M. McCaskey, M. Ramsey-Musolf and G. Shaughnessy, Phys. Rev. D **79** (2009) 015018 [arXiv:0811.0393 [hep-ph]].
- [19] M. Pospelov, A. Ritz and M. B. Voloshin, Phys. Lett. B **662** (2008) 53 [arXiv:0711.4866 [hep-ph]].
- [20] M. R. Buckley, D. Feld and D. Goncalves, arXiv:1410.6497 [hep-ph].
- [21] D. S. Akerib *et al.* [LUX Collaboration], Phys. Rev. Lett. **112** (2014) 091303 [arXiv:1310.8214 [astro-ph.CO]].
- [22] E. Aprile *et al.* [XENON100 Collaboration], Phys. Rev. Lett. **109** (2012) 181301 [arXiv:1207.5988 [astro-ph.CO]].
- [23] M. Beltran, D. Hooper, E. W. Kolb, Z. A. C. Krusberg and T. M. P. Tait, JHEP **1009** (2010) 037 [arXiv:1002.4137 [hep-ph]].
- [24] J. Goodman, M. Ibe, A. Rajaraman, W. Shepherd, T. M. P. Tait and H. B. Yu, Phys. Rev. D **82** (2010) 116010 [arXiv:1008.1783 [hep-ph]].
- [25] Y. Bai, P. J. Fox and R. Harnik, JHEP **1012** (2010) 048 [arXiv:1005.3797 [hep-ph]].
- [26] G. Belanger, B. Dumont, U. Ellwanger, J. F. Gunion and S. Kraml, Phys. Lett. B **723** (2013) 340 [arXiv:1302.5694 [hep-ph]].
- [27] C. Boehm, M. J. Dolan, C. McCabe, M. Spannowsky and C. J. Wallace, JCAP **1405** (2014) 009 [arXiv:1401.6458 [hep-ph]].
- [28] A. Berlin, D. Hooper and S. D. McDermott, Phys. Rev. D **89** (2014) 115022 [arXiv:1404.0022 [hep-ph]].
- [29] C. Boehm, M. J. Dolan and C. McCabe, Phys. Rev. D **90** (2014) 023531 [arXiv:1404.4977 [hep-ph]].
- [30] P. Ko, W. I. Park and Y. Tang, JCAP **1409** (2014) 013 [arXiv:1404.5257 [hep-ph]].

- [31] M. Abdullah, A. DiFranzo, A. Rajaraman, T. M. P. Tait, P. Tanedo and A. M. Wijangco, Phys. Rev. D **90** (2014) 3, 035004 [arXiv:1404.6528 [hep-ph]].
- [32] A. Berlin, P. Gratia, D. Hooper and S. D. McDermott, Phys. Rev. D **90** (2014) 015032 [arXiv:1405.5204 [hep-ph]].
- [33] J. M. Cline, G. Dupuis, Z. Liu and W. Xue, JHEP **1408** (2014) 131 [arXiv:1405.7691 [hep-ph]].
- [34] L. Wang, arXiv:1406.3598 [hep-ph].
- [35] C. Cheung, M. Papucci, D. Sanford, N. R. Shah and K. M. Zurek, Phys. Rev. D **90** (2014) 075011 [arXiv:1406.6372 [hep-ph]].
- [36] C. Balzs and T. Li, Phys. Rev. D **90** (2014) 055026 [arXiv:1407.0174 [hep-ph]].
- [37] J. Huang, T. Liu, L. T. Wang and F. Yu, Phys. Rev. D **90** (2014) 115006 [arXiv:1407.0038 [hep-ph]].
- [38] K. Ghorbani, JCAP **1501** (2015) 015 [arXiv:1408.4929 [hep-ph]].
- [39] A. D. Banik and D. Majumdar, arXiv:1408.5795 [hep-ph].
- [40] D. Borah and A. Dasgupta, arXiv:1409.1406 [hep-ph].
- [41] M. Cahill-Rowley, J. Gainer, J. Hewett and T. Rizzo, arXiv:1409.1573 [hep-ph].
- [42] J. Guo, J. Li, T. Li and A. G. Williams, arXiv:1409.7864 [hep-ph].
- [43] M. J. Dolan, C. McCabe, F. Kahlhoefer and K. Schmidt-Hoberg, arXiv:1412.5174 [hep-ph].
- [44] A. Biswas, arXiv:1412.1663 [hep-ph].
- [45] J. Cao, L. Shang, P. Wu, J. M. Yang and Y. Zhang, arXiv:1410.3239 [hep-ph].
- [46] N. F. Bell, S. Horiuchi and I. M. Shoemaker, Phys. Rev. D **91** (2015) 023505 [arXiv:1408.5142 [hep-ph]].
- [47] W. Detmold, M. McCullough and A. Pochinsky, Phys. Rev. D **90** (2014) 11, 115013 [arXiv:1406.2276 [hep-ph]].
- [48] K. Cheung, W. C. Huang and Y. L. S. Tsai, arXiv:1411.2619 [hep-ph].
- [49] P. Ko and Y. Tang, JCAP **1501** (2015) 023 [arXiv:1407.5492 [hep-ph]].
- [50] J. D. Ruiz-Alvarez, C. A. de S.Pires, F. S. Queiroz, D. Restrepo and P. S. Rodrigues da Silva, Phys. Rev. D **86** (2012) 075011 [arXiv:1206.5779 [hep-ph]].
- [51] T. Basak and T. Mondal, arXiv:1405.4877 [hep-ph].
- [52] G. Marshall and R. Primulando, JHEP **1105** (2011) 026 [arXiv:1102.0492 [hep-ph]].
- [53] N. Okada and O. Seto, Phys. Rev. D **89** (2014) 043525 [arXiv:1310.5991 [hep-ph]].
- [54] J. Liu, N. Weiner and W. Xue, arXiv:1412.1485 [hep-ph].
- [55] M. Freytsis, D. J. Robinson and Y. Tsai, arXiv:1410.3818 [hep-ph].

- [56] T. Lacroix, C. Boehm and J. Silk, Phys. Rev. D **90** (2014) 4, 043508 [arXiv:1403.1987 [astro-ph.HE]].
- [57] P. Agrawal, B. Batell, P. J. Fox and R. Harnik, arXiv:1411.2592 [hep-ph].
- [58] F. Calore, I. Cholis and C. Weniger, arXiv:1409.0042 [astro-ph.CO].
- [59] F. Calore, I. Cholis, C. McCabe and C. Weniger, arXiv:1411.4647 [hep-ph].
- [60] S. Heinemeyer *et al.* [LHC Higgs Cross Section Working Group Collaboration], arXiv:1307.1347 [hep-ph].
- [61] A. Belyaev, N. D. Christensen and A. Pukhov, Comput. Phys. Commun. **184** (2013) 1729 [arXiv:1207.6082 [hep-ph]].
- [62] A. Semenov, arXiv:1005.1909 [hep-ph].
- [63] G. Belanger, F. Boudjema, A. Pukhov and A. Semenov, Comput. Phys. Commun. **185** (2014) 960 [arXiv:1305.0237 [hep-ph]].
- [64] K. Griest and D. Seckel, Phys. Rev. D **43** (1991) 3191.
- [65] J. Edsjo, M. Schelke, P. Ullio and P. Gondolo, JCAP **0304** (2003) 001 [hep-ph/0301106].
- [66] S. Profumo and A. Provenza, JCAP **0612** (2006) 019 [hep-ph/0609290].
- [67] D. Hooper and S. Profumo, Phys. Rept. **453** (2007) 29 [hep-ph/0701197].
- [68] G. Servant and T. M. P. Tait, Nucl. Phys. B **650** (2003) 391 [hep-ph/0206071].
- [69] K. Kong and K. T. Matchev, JHEP **0601** (2006) 038 [hep-ph/0509119].
- [70] F. Burnell and G. D. Kribs, Phys. Rev. D **73** (2006) 015001 [hep-ph/0509118].
- [71] M. Klasen, C. E. Yaguna, J. D. Ruiz-Alvarez, D. Restrepo and O. Zapata, JCAP **1304** (2013) 044 [arXiv:1302.5298 [hep-ph]].
- [72] G. Belanger, F. Boudjema, A. Pukhov and A. Semenov, Comput. Phys. Commun. **180** (2009) 747 [arXiv:0803.2360 [hep-ph]].
- [73] J. R. Ellis, K. A. Olive and C. Savage, Phys. Rev. D **77** (2008) 065026 [arXiv:0801.3656 [hep-ph]].
- [74] T. Nihei and M. Sasagawa, Phys. Rev. D **70** (2004) 055011 [Erratum-ibid. D **70** (2004) 079901] [hep-ph/0404100].
- [75] J. R. Ellis, A. Ferstl and K. A. Olive, Phys. Lett. B **481** (2000) 304 [hep-ph/0001005].
- [76] A. Crivellin, M. Hoferichter and M. Procura, Phys. Rev. D **89** (2014) 054021 [arXiv:1312.4951 [hep-ph]].
- [77] B. Batell, M. Pospelov and A. Ritz, Phys. Rev. D **79** (2009) 115019 [arXiv:0903.3396 [hep-ph]].
- [78] R. Rando [Fermi LAT Collaboration], arXiv:0907.0626 [astro-ph.IM].
- [79] Fermi-LAT Collaboration, S. Murgia, “Observation of the High Energy Gamma-ray Emission Towards the Galactic Center”. <http://fermi.gsfc.nasa.gov/science/mtgs/symposia/2014/program/08-Murgia.pdf>, (October 2014).

- [80] L. Goodenough and D. Hooper, arXiv:0910.2998 [hep-ph].
- [81] D. Hooper and L. Goodenough, Phys. Lett. B **697** (2011) 412 [arXiv:1010.2752 [hep-ph]].
- [82] A. Boyarsky, D. Malyshev and O. Ruchayskiy, Phys. Lett. B **705** (2011) 165 [arXiv:1012.5839 [hep-ph]].
- [83] D. Hooper and T. Linden, Phys. Rev. D **84** (2011) 123005 [arXiv:1110.0006 [astro-ph.HE]].
- [84] K. N. Abazajian and M. Kaplinghat, Phys. Rev. D **86** (2012) 083511 [arXiv:1207.6047 [astro-ph.HE]].
- [85] D. Hooper and T. R. Slatyer, Phys. Dark Univ. **2** (2013) 118 [arXiv:1302.6589 [astro-ph.HE]].
- [86] C. Gordon and O. Macias, Phys. Rev. D **88** (2013) 083521 [Erratum-ibid. D **89** (2014) 4, 049901] [arXiv:1306.5725 [astro-ph.HE]].
- [87] K. N. Abazajian, N. Canac, S. Horiuchi and M. Kaplinghat, Phys. Rev. D **90** (2014) 023526 [arXiv:1402.4090 [astro-ph.HE]].
- [88] T. Daylan, D. P. Finkbeiner, D. Hooper, T. Linden, S. K. N. Portillo, N. L. Rodd and T. R. Slatyer, arXiv:1402.6703 [astro-ph.HE].
- [89] B. Zhou, Y. F. Liang, X. Huang, X. Li, Y. Z. Fan, L. Feng and J. Chang, arXiv:1406.6948 [astro-ph.HE].
- [90] D. Hooper, I. Cholis, T. Linden, J. Siegal-Gaskins and T. Slatyer, Phys. Rev. D **88** (2013) 083009 [arXiv:1305.0830 [astro-ph.HE]].
- [91] T. Linden, E. Lovegrove and S. Profumo, Astrophys. J. **753** (2012) 41 [arXiv:1203.3539 [astro-ph.HE]].
- [92] J. F. Navarro, C. S. Frenk and S. D. M. White, Astrophys. J. **462** (1996) 563 [astro-ph/9508025].